Hindawi Publishing Corporation
Abstract and Applied Analysis
Volume 2012, Article ID 414060, 26 pages
doi:10.1155/2012/414060

Research Article

q-Advanced Models for Tsunami and Rogue Waves

D. W. Pravica, N. Randriampiry, and M. J. Spurr

Department of Mathematics, East Carolina University, Greenville, NC 27858, USA

Correspondence should be addressed to M. J. Spurr, spurrm@ecu.edu

Received 9 March 2012; Revised 19 May 2012; Accepted 21 May 2012

Academic Editor: Ferhan M. Atici

A wavelet $K_q(t)$, that satisfies the q-advanced differential equation $K_q'(t) = K_q(qt)$ for $q > 1$, is used to model N-wave oscillations observed in tsunamis. Although q-advanced ODEs may seem nonphysical, we present an application that model tsunamis, in particular the Japanese tsunami of March 11, 2011, by utilizing a one-dimensional wave equation that is forced by $F_q(t,x) = K_q(t)\,{}_q\mathrm{Sin}(x)$. The profile F_q is similar to tsunami models in present use. The function ${}_q\mathrm{Sin}(t)$ is a wavelet that satisfies a q-advanced harmonic oscillator equation. It is also shown that another wavelet, ${}_q\mathrm{Cos}(t)$, matches a rogue-wave profile. This is explained in terms of a resonance wherein two small amplitude forcing waves eventually lead to a large amplitude rogue. Since wavelets are used in the detection of tsunamis and rogues, the signal-analysis performance of K_q and ${}_q\mathrm{Cos}$ is examined on actual data.

1. Introduction

Tsunami or maremoto waves occur in response to earthquakes or landslides on the seafloor of large bodies of water, as discussed in [1–4]. The consequential runup to the shore is such that the tide goes out, then returns as a large surge, only to be followed by several diminishing cycles of similar events [5]. An understanding of this behavior involves a consideration of the effects from the seafloor near the shore where the wave velocity decreases [6, 7]. We study a short-lived forcing that predominantly generates a traveling-wave profile $K_q(x - ct)$ where K_q solves a multiplicatively advanced differential equation (MADE) whose profile resembles a typical tsunami (see Figure 1). In contrast to the N-wave profile proposed in [8], the K_q-MADE profiles are asymmetric wavelets that are flat on a half-line.

In an apparently unrelated phenomena, rogue, freak, or monster waves are caused by small ripples or currents in layers near the water's surface [9, 10]. Various methods have been used to model these rare events, as in [11, 12]. Here, we demonstrate why rogue waves may be a type of resonance wherein an arbitrarily low amplitude forcing, for a sufficiently long period of time, can produce any size of localized wave. Our models use

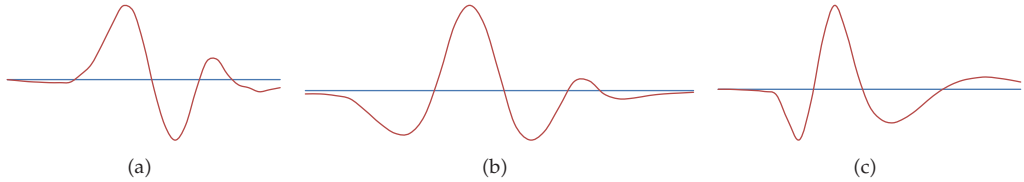

Figure 1: (a) Tsunami 52406 from DART, March 2011; (b) replica of tsunami-model profile adapted from [7]; (c) MADE solution profile $y = K_q(t)$ for $q = 1.5$.

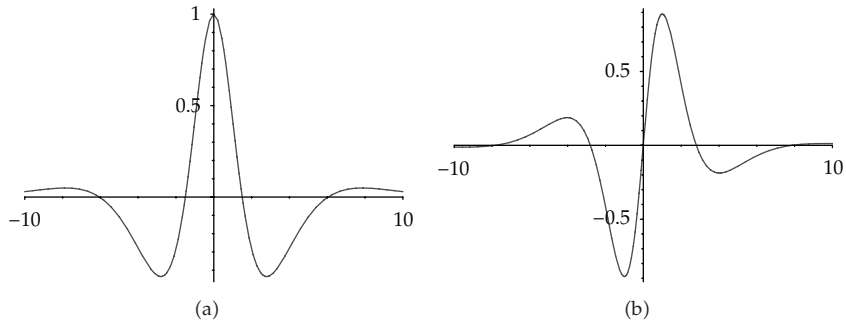

Figure 2: (a) $y = {}_q\mathrm{Cos}(t)$ for $q = 1.5$; and (b) $y = {}_q\mathrm{Sin}(t)$ for $q = 1.5$.

square-integrable versions of the sine and cosine functions that we call ${}_q\mathrm{Cos}(t)$ and ${}_q\mathrm{Sin}(t)$ (see Figure 2).

Tsunami and rogue waves are perturbations of the water-surface elevation function $\eta(t, x, y)$. The surface velocity components $\mathbf{U} \equiv (u, v, w)$ are small and the time-averaged mean-flow velocity $\langle \mathbf{U} \rangle$ is assumed to remain $\mathbf{0}$ everywhere. Subject to assumptions, the functions K_q, ${}_q\mathrm{Cos}$ and ${}_q\mathrm{Sin}$ will be used in the construction of the forcing terms in the Matsuno equations [13] as given by

$$\begin{aligned}
\frac{\partial u}{\partial t} + u\frac{\partial u}{\partial x} + v\frac{\partial u}{\partial y} - f_0 v &= -\alpha(u,v)u - g_0\left(\frac{\partial \eta}{\partial x}\right) + P_x,\\
\frac{\partial v}{\partial t} + u\frac{\partial v}{\partial x} + v\frac{\partial v}{\partial y} + f_0 u &= -\alpha(u,v)v - g_0\left(\frac{\partial \eta}{\partial y}\right) + P_y,\\
w + \frac{\partial}{\partial x}\left[(H+\eta)u\right] + \frac{\partial}{\partial y}\left[(H+\eta)v\right] &= -\alpha(u,v)\eta + Q,
\end{aligned} \tag{1.1}$$

where $H(x, y)$ is the depth of the water, $w \equiv \partial\eta/\partial t$ is the vertical velocity of the wave surface, P_x and P_y are variable external forcings, and Q is a mass source term. The acceleration due to gravity g_0 accounts for buoyancy, and the Coriolis parameter f_0 addresses the rotation of the earth (only required for very long waves over the earth [14]). The friction coefficient $\alpha \geq 0$ acts as a generic sink that reduces the amplitude over time [6].

This work considers localized plane waves, or wavelets, on a flat sea propagating only in the x-direction. Thus, we set

$$u = u(t,x), \qquad w = w(t,x), \qquad \eta = \eta(t,x), \qquad v(t,x,y) = 0,$$
$$H = H(x), \qquad c = c(x) \equiv \sqrt{g_0 H(x)}, \tag{1.2}$$
$$P_x = P_x(t,x), \qquad \alpha = f_0 = P_y = Q = 0.$$

In deep water $H = H_0 > 0$ is a fixed constant and $c_0 = \sqrt{g_0 H_0}$ is a constant surface-wave speed (called the celerity). Then, for small amplitudes, the elevation function $\eta(t,x)$ satisfies

$$\text{generation: } \frac{\partial^2 \eta}{\partial t^2} - c_0^2 \frac{\partial^2 \eta}{\partial x^2} = F(t,x), \quad \text{where } \eta(t,x) \simeq 0, \text{ for } t \ll 0, \ x \in \mathbb{R}, \tag{1.3}$$

$$\text{propagation: } \frac{\partial \eta}{\partial t} + c_0 \frac{\partial}{\partial x}\left(\eta + \frac{\beta}{c_0}\eta^2 + \frac{\nu}{c_0}\frac{\partial^2 \eta}{\partial x^2}\right) = 0, \quad \text{for } H(x) \simeq H_0, \tag{1.4}$$

$$\text{runup: } \frac{\partial \eta}{\partial t} + c\frac{\partial \eta}{\partial x} + \frac{\eta}{2}\frac{dc}{dx} + \beta\frac{\partial(\eta^2)}{\partial x} + \nu\frac{\partial^3 \eta}{\partial x^3} = 0, \quad \text{for } H(x) > 0. \tag{1.5}$$

These equations are found in [8, Equation (2)], [15, Equation (45)], and [16, Equation (13)], respectively. The new coefficients are defined as $\beta(x) \equiv 3c/(4H)$ and $\nu(x) \equiv cH^2/6$. Equation (1.4) is referred to as the KdV-top model in [16]. Inclusion of an additional boundary-turbulence term in (1.5) would result in a loss of conservation properties for η (considered in [17] but not here).

The forcings $F(t,x)$ in (1.3) will be constructed from bounded wavelets $\phi(u)$ that satisfy MADEs. As such they satisfy the following conditions:

$$\phi \in \mathcal{L}^1(\mathbb{R}) \cap \mathcal{L}^2(\mathbb{R}) \cap \mathcal{L}^\infty(\mathbb{R}), \qquad \int_{-\infty}^{\infty} \phi(u)du = 0. \tag{1.6}$$

Physically, if ϕ represents the displacement of the water-level from equilibrium, conservation of mass necessitates that the conditions in (1.6) hold. Note that, as discussed in [15], solitons are not expected to occur in (1.4) since the total spatial integral of η vanishes. We find that if $F(t_*,x)$ is a wavelet in the x variable (for fixed $t_* \in \mathbb{R}$), then so is $\eta(t_*,x)$ away from the shore (using x-integration of either (1.3) or (1.4)). During the runup, however, $\eta(t,x)$ looses its wavelet properties due to the variability of the coefficients in (1.5).

It seems natural that wavelets should appear in the study of surface water waves. The wavelets presented here are particularly well suited for surface waves. In particular, we show that when the forcing F is expressed in terms of K_q, ${}_q\mathrm{Cos}$ and ${}_q\mathrm{Sin}$ in (2.2)-(2.3), the solution can be reexpressed in terms of these functions. An objective of this paper is to demonstrate that the modeling as well as the detection and analysis of an observed wave profile can be achieved efficiently in terms of the wavelets (2.2)-(2.3), see [18–20]. Hence, a brief discussion on the topics of signal analysis and recovery on real data is presented using K_q and ${}_q\mathrm{Cos}$. We apply these techniques to the Japanese tsunami of March 11, 2011. The paper is completed with the details of a perturbation analysis in $q > 1^+$ that is needed to establish the existence of a resonance for rogue waves.

2. Preliminaries on Special Functions

The first quantity that we introduce is the function $K_q(t)$ that satisfies the MADE

$$K_q'(t) = K_q(qt), \quad \forall t \in \mathbb{R},\ q > 1. \tag{2.1}$$

We set $K_q(t) \equiv 0$ for $t \le 0$, and define

$$K_q(t) \equiv \sum_{j=-\infty}^{\infty} \frac{(-1)^j e^{-q^j t}}{q^{j(j+1)/2}}, \quad \text{for } t > 0,\ q > 1. \tag{2.2}$$

Note that $K_q(t)$ satisfies the wavelet conditions in (1.6), see [18]. Furthermore, as in [20], the reproducing kernel of $K_q(t)$ gives the functions

$$\begin{aligned} {}_q\mathrm{Cos}(t) &= N_q \cdot \int_0^{\infty} K_q(u) K_q(u-t)\,du = N_q \sum_{j=-\infty}^{\infty} \frac{(-1)^j e^{-q^{2j}|t|}}{q^{j^2}}, \\ {}_q\mathrm{Sin}(t) &= -N_q \cdot \int_0^{\infty} K_q(u) K_q(qu-qt)\,du = \left(\frac{t}{|t|}\right) N_q \sum_{j=-\infty}^{\infty} \frac{(-1)^j e^{-q^{2j}|t|}}{q^{j(j-1)}}, \end{aligned} \tag{2.3}$$

which are displayed in Figure 2 for $q = 1.5$. The normalization constant N_q is chosen so that ${}_q\mathrm{Cos}\,(0) = 1$. It is shown in [20] that the q-advanced harmonic oscillator equations,

$${}_q\mathrm{Cos}''(t) = -q \cdot {}_q\mathrm{Cos}(qt), \qquad {}_q\mathrm{Sin}''(t) = -q^2 \cdot {}_q\mathrm{Sin}(qt), \tag{2.4}$$

hold, which are second-order MADEs. Each of (2.2)-(2.3) lies in $\mathcal{L}^2$. We show as a consequence of Theorem 2.1 that ${}_q\mathrm{Cos}(t) \to \cos(t)$ and ${}_q\mathrm{Sin}(t) \to \mathrm{Sin}(t)$ pointwise for $t \in \mathbb{R}$ as $q \to 1^+$. Note, we also have uniform convergence on compact sets, which was obtained in [20]. Thus, ${}_q\mathrm{Cos}(t)$ and ${}_q\mathrm{Sin}(t)$ can be viewed as $\mathcal{L}^2$ approximations of $\cos(t)$ and $\sin(t)$, respectively, which are solutions of the limit of equations in (2.4) as $q \to 1^+$.

2.1. Theta Functions

As part of our study, we employ the Jacobi theta function, defined for $\omega \in \mathbb{C} \setminus \{-q^n\}_{n\in\mathbb{Z}}$,

$$\begin{aligned} \theta(q,\omega) &\equiv \sum_{k=-\infty}^{\infty} \frac{\omega^k}{q^{k(k-1)/2}} = \mu_q \prod_{n=0}^{\infty} \left(1 + \frac{\omega}{q^n}\right)\left(1 + \frac{1}{\omega q^{n+1}}\right), \\ \mu_q &\equiv \prod_{n=0}^{\infty} \left(1 - \frac{1}{q^{n+1}}\right). \end{aligned} \tag{2.5}$$

This function will only be used in regions where $\omega > 0$ and $q > 1$. Clearly the function $\theta(q^2, \omega^2)$ is C^∞ for all $\omega \in \mathbb{R} - \{0\}$ and grows faster than any rational polynomial at $\pm\infty$ and 0.

As such, for each $q > 1$ one has that $1/\theta(q^2, \omega^2)$ is a Schwartz function that is flat at $\omega = 0$. It also satisfies the algebraic identity

$$\theta(q; q^n\omega) = q^{n(n+1)/2}\omega^n\theta(q;\omega), \quad n \in \mathbb{Z}, \tag{2.6}$$

which plays an important role in our analysis, [18].

Theorem 2.1. *For $q > 1$, let*

$$\delta_q(\omega) \equiv \begin{cases} \dfrac{1}{[\ln(q)\theta(q^2;\omega^2)]} & \text{if } \omega > 0 \\ 0 & \text{if } \omega \le 0. \end{cases} \tag{2.7}$$

Then $\delta_q(\omega)$ is a delta sequence in $q > 1^+$, at $\omega = 1$ and has the following properties:

$$\text{(i)} \lim_{q\to 1^+} \delta_q(\omega \neq 1) = 0, \qquad \text{(ii)} \lim_{q\to 1^+} \delta_q(1) = \infty, \qquad \text{(iii)} \lim_{q\to 1^+} \int_0^\infty \delta_q(\omega)d\omega = 1. \tag{2.8}$$

Proof. From [21], for $1 < q < e^\pi$ and for $\omega > 0$ one has

$$0 < q^{1/4}|\omega|e^{(\ln(|\omega|))^2/\ln(q)}\left\{\sqrt{\frac{\pi}{\ln(q)}} - 1\right\} \le \theta\left(q^2;\omega^2\right), \tag{2.9}$$

$$0 < \theta\left(q^2;\omega^2\right) \le q^{1/4}|\omega|e^{(\ln(|\omega|))^2/\ln(q)}\left\{\sqrt{\frac{\pi}{\ln(q)}} + 1\right\}. \tag{2.10}$$

Multiplication of (2.9) and (2.10) by $\ln(q)$, followed by reciprocation, gives that for $\omega > 0$

$$\left[\frac{q^{-1/4}|\omega|^{-1}e^{-(\ln(|\omega|))^2/\ln(q)}}{\sqrt{\ln(q)}\left\{\sqrt{\pi} + \sqrt{\ln(q)}\right\}}\right] \le \delta_q(\omega) \le \left[\frac{q^{-1/4}|\omega|^{-1}e^{-(\ln(|\omega|))^2/\ln(q)}}{\sqrt{\ln(q)}\left\{\sqrt{\pi} - \sqrt{\ln(q)}\right\}}\right]. \tag{2.11}$$

Now, (i) follows from (2.11) and the fact that for $k > 0$, $\lim_{q\to 1^+}[e^{-k/\ln(q)}/\sqrt{\ln(q)}] = 0$. For $\omega = 1$, (ii) also follows from (2.11). To obtain (iii), we handle some preliminaries. First, it was shown in [18] that

$$\begin{aligned} \|K_q\|_2^2 &\equiv \int_{-\infty}^{\infty} |K_q(t)|^2 dt = \int_{-\infty}^{\infty} \frac{q^2(\mu_q)^4\mu_{q^2}}{2\pi\theta(q^2;q^2\omega^2)}d\omega \\ &= \frac{q(\mu_q)^4\mu_{q^2}}{2\pi}\int_{-\infty}^{\infty}\frac{dv}{\theta(q^2;v^2)} = \frac{q(\mu_q)^4\mu_{q^2}}{\pi}\int_0^\infty \frac{dv}{\theta(q^2;v^2)}. \end{aligned} \tag{2.12}$$

The functional identity $(\mu_q)^4 q = 2\|K_q\|_2^2 (\mu_{q^2})^2 N_q$, established in [20], allows for the replacement of $(\|K_q\|_2^2/q)$ by $((\mu_q)^4/[2(\mu_{q^2})^2 N_q])$ in (2.12) to obtain the following:

$$\int_0^\infty \frac{dv}{\theta(q^2;v^2)} = \frac{\pi \|K_q\|_2^2}{q(\mu_q)^4 \mu_{q^2}} = \frac{\pi}{2N_q(\mu_{q^2})^3}. \tag{2.13}$$

This in turn gives that

$$\lim_{q\to 1^+} \int_0^\infty \delta_q(\omega)d\omega = \lim_{q\to 1^+} \int_0^\infty \frac{d\omega}{\ln(q)\theta(q^2;\omega^2)} = \lim_{q\to 1^+} \frac{\pi}{2\ln(q)N_q(\mu_{q^2})^3} = 1, \tag{2.14}$$

where the last equality follows from the q-Wallis limit, $\lim_{q\to 1^+}[\ln(q)N_q(\mu_{q^2})^3] = \pi/2$, from [21]. This proves (iii) and finishes the proof of the theorem. □

2.2. q-Advanced Wavelets That Solve MADEs

The appearance of theta functions is a consequence of the Laplace transform of (2.2),

$$K_q(t) = \mathcal{L}^{-1}\left[\frac{-\mu_q^3}{s\theta(q,s)}\right](t), \quad \text{where } \mathcal{L}[f(t)](s) \equiv \int_{t=0}^\infty e^{-st} f(t)dt. \tag{2.15}$$

In [20], we use the inverse Fourier transform to compute the expressions

$$\begin{aligned} {}_q\mathrm{Cos}(t) &= \frac{(\mu_{q^2})^3 N_q}{\pi} \int_{-\infty}^\infty \frac{e^{i\omega t}d\omega}{\theta(q^2,\omega^2)}, \\ {}_q\mathrm{Sin}(t) &= \frac{-i(\mu_{q^2})^3 N_q}{\pi} \int_{-\infty}^\infty \frac{e^{i\omega t}\omega d\omega}{\theta(q^2,\omega^2)}, \end{aligned} \tag{2.16}$$

and these expressions will be used in the proof of a resonance for rogue waves. The representation in (2.15) verifies the MADE in (2.1), and (2.16) implies the identities

$${}_q\mathrm{Cos}'(t) = -{}_q\mathrm{Sin}(t), \qquad {}_q\mathrm{Sin}'(t) = q\cdot {}_q\mathrm{Cos}(qt), \tag{2.17}$$

which verify the MADEs in (2.4). Now Theorem 2.1 gives that both $\delta_q(\omega)$ and $\delta_q(-\omega)$ are delta sequences in $q > 1^+$ at $\omega = \pm 1$, respectively. These applied to (2.16), in combination with the q-Wallis limit, give that pointwise

$$\lim_{q\to 1^+} {}_q\mathrm{Cos}(t) = \cos(t), \quad \lim_{q\to 1^+} {}_q\mathrm{Sin}(t) = \sin(t), \quad \text{for } t \in \mathbb{R}. \tag{2.18}$$

For $q > 1$, the functions in (2.15) and (2.16) are in the Schwartz space. In particular, their rates of decay for large $|t|$ are typically slower than exponential but faster than any reciprocal polynomial. It can be shown that $\exists C > 0$ so that for $t \in \mathbb{R}$ and $q > 1$,

$$\max\left\{ \left|K_q(t)\right|, \left|{}_q\mathrm{Cos}(t)\right|, \left|{}_q\mathrm{Sin}(t)\right|, \frac{1}{\left|\theta(q;t)\right|} \right\} \leq Cq^{-\log_q^2(|t|)}. \tag{2.19}$$

Remark 2.2. The use of theta functions in frequency space provides decaying versions of *cosine* and *sine* while preserving many differential properties of these functions.

3. Tsunami Modeling Using MADEs

A tsunami wave is the consequence of a spontaneous change in elevation on the seafloor, which creates a variable pressure field throughout the volume of water. This sets up forces that extend to the surface of the ocean causing it to be moved up and down, locally. The perturbed wave height then propagates away from this disturbance. In still water, the surface wave speed $c_0 = \sqrt{g_0 H_0}$ mainly depends on the average depth H_0 of the ocean. For tsunamis, the wavelength is much longer than H_0 and so the shallow-water wave equation applies (see [22, page 195]). Near the shore nonlinear effects need to be introduced to account for the sloping of the shoreline [4, 12, 23, 24].

Suppose that the faultline on the seafloor is parallel to the y coordinate. Then the y-dependence can be ignored even after the tsunami-causing event has taken place. In this situation, the wave front will travel in the x direction only.

3.1. q-Advanced Tsunami Model

Consider the forced one-dimensional wave equation for the water-level function ψ [14, 22],

$$\partial_t^2\psi(t,x) - c_0^2\partial_x^2\psi(t,x) = F(t,x), \quad \forall t \in \mathbb{R},\ x \in \mathbb{R}, \qquad \psi(t,x) = 0, \quad \forall t < 0,\ x \in \mathbb{R}, \tag{3.1}$$

where the condition on the right in (3.1) constitutes the boundary and initial conditions. The forcing is expected to satisfy the conditions, for fixed $t_*, x_* \in \mathbb{R}$,

$$\lim_{|t|\to\infty} F(t,x_*) = 0, \qquad \lim_{|x|\to\infty} F(t_*,x) = 0, \qquad \int_{-\infty}^{\infty} F(t_*,x)dx = 0, \tag{3.2}$$

and is related to the depth of the ocean floor by $\partial_t^2 H(t,x) = F(t,x)$. The models in [4, 8] start with ground-motion profiles $H = H_{\mathrm{TS}}$ or $H = H_{\mathrm{ZWL}}$ where

$$H_{\mathrm{TS}} \equiv \frac{A}{\gamma}\tanh\left(\gamma x - \frac{t}{\tau}\right), \qquad H_{\mathrm{ZWL}} \equiv (2A\gamma)\mathrm{sech}^2(\gamma x)\tanh(\gamma x)\sin\left(\frac{\pi t}{2\tau}\right), \tag{3.3}$$

respectively. In [8], it is noted that using the first model $H = H_{\mathrm{TS}}$ gives a force consistent with a landslide that continues for all time. In [4], the second model $H = H_{\mathrm{ZWL}}$ suggests an earthquake that continues for all time. In these settings, (3.2) does not hold. However, these

models are still used as part of the initial forcings for the wave equation since they lead to integrable solutions whose evolutions resemble that of actual tsunamis. As a comparison, we propose the following q-advanced model:

$$\begin{aligned} H_q(t,x) &\equiv \quad A \cdot K_q\left(\frac{t}{\tau}\right)_q \mathrm{Sin}(\gamma \cdot x), \\ F_q(t,x) \equiv \frac{\partial^2 H_q}{\partial t^2} &= \frac{A \cdot q}{\tau^2} \quad K_q\left(\frac{q^2 t}{\tau}\right)_q \mathrm{Sin}(\gamma \cdot x), \end{aligned} \tag{3.4}$$

where $F_q(t,x)$ now satisfies the conditions in (3.2). When (3.4) is substituted into (3.1), solved and simplified, one obtains a unique solution $\psi(t,x)$ to the forced wave equation. To express the solution, define the two phase functions, corresponding to right and left propagation,

$$\varphi_\mu^+(t,x,\xi) \equiv \frac{t}{\tau} - \frac{\gamma \cdot x - \xi}{q^\mu}, \qquad \varphi_\mu^-(t,x,\xi) \equiv \frac{t}{\tau} + \frac{\gamma \cdot x - \xi}{q^\mu}, \quad \forall t,x,\xi \in \mathbb{R}, \tag{3.5}$$

where the parameters are related by $c_0 \gamma \tau = q^\mu$. Define, for any $\alpha, \beta, \mu \in \mathbb{R}$ and $q > 1$,

$$\mathcal{T}_{\alpha,\beta,\mu}^{\pm}(t,x) \equiv \int_{\xi=0}^{\gamma \cdot x} {}_q\mathrm{Sin}\left(q^\alpha \cdot \xi\right) \cdot K_q\left(q^\beta \cdot \varphi_\mu^{\pm}(t,x,\xi)\right) d\xi. \tag{3.6}$$

Then, for $t > 0$ and $x \in \mathbb{R}$, the reader can verify that

$$\psi(t,x) = \psi_{\text{particular}}(t,x) + \psi_{\text{homogeneous}}(t,x), \tag{3.7}$$

where a particular solution to (3.1), with the forcing in (3.4), is

$$\psi_{\text{particular}}(t,x) \;= \left(\frac{-A \cdot q^{-\mu}}{2}\right) \cdot \left[\mathcal{T}_{0,1,\mu}^{-}(t,x) \;-\; \mathcal{T}_{0,1,\mu}^{+}(t,x)\right]. \tag{3.8}$$

A smooth solution that satisfies $\psi(t,x) = 0$, for $t \leq 0$, is obtained by choosing

$$\psi_{\text{hom.}}(t,x) = \frac{-1}{2}\left[\psi_{\text{par.}}(0, x + c_0 t) + \psi_{\text{par.}}(0, x - c_0 t) + \int_{x-c_0 t}^{x+c_0 t} \frac{\partial \psi_{\text{par.}}(0,u)}{c_0 \cdot \partial t} du\right]. \tag{3.9}$$

One can see from (3.5)–(3.9) that the solution has the basic wavelet properties

$$\psi(\cdot, x_*), \psi(t_*, \cdot) \in \mathcal{L}^1(\mathbb{R}) \cap \mathcal{L}^2(\mathbb{R}) \cap \mathcal{L}^\infty(\mathbb{R}), \qquad \int_{\mathbb{R}} \psi(t, x_*) dt = \int_{\mathbb{R}} \psi(t_*, x) dx = 0, \tag{3.10}$$

for each $t_*, x_* \in \mathbb{R}$. To analyze the long-term behavior of the solution ψ, we use (2.1), (2.17), and integration by parts, twice, to obtain Proposition 3.1.

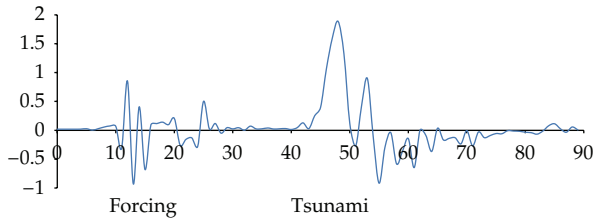

Figure 3: DART 21418: Data showing earthquake (*forcing*, on the left) and resulting *tsunami* (on the right) observed on March 11, 2011, from 5:43 am to 6:51 am (horizontal axis is time in minutes, vertical axis is in meters).

Proposition 3.1. *For any* $\alpha, \beta, \mu \in \mathbb{R}$ *and* $q > 1$ *the following identity holds:*

$$\begin{aligned}\mathcal{T}^{\pm}_{\alpha,\beta,\mu}(t,x) &= q^{-\alpha}\cdot K_q\left(q^{\beta}\cdot\left[\frac{t}{\tau}\mp\frac{\gamma x}{q^{\mu}}\right]\right) - q^{-2\alpha+2\beta-2\mu+1}\cdot\mathcal{T}^{\pm}_{\alpha-1,\beta+2,\mu}(t,x)\\ &\quad - q^{-\alpha}\cdot {}_q\mathrm{Cos}\left(q^{\alpha}\gamma x\right)\cdot K_q\left(\frac{q^{\beta}t}{\tau}\right)\pm q^{-2\alpha+\beta-\mu}\,{}_q\mathrm{Sin}\left(q^{\alpha-1}\gamma x\right)\cdot K_q\left(\frac{q^{\beta+1}t}{\tau}\right).\end{aligned} \tag{3.11}$$

The expression in (3.11) demonstrates that $\mathcal{T}^{\pm}_{\alpha,\beta,\mu}$, as used in (3.8), can be written as a series of localized (bound) states and traveling (free) states. These different terms appear as translated and scaled versions of the wavelets K_q, ${}_q\mathrm{Cos}$ and ${}_q\mathrm{Sin}$. Thus, such functions provide a good match for a wave profile ψ that was generated by the family of forcings F_q in (3.4). Furthermore, for $t \gg 0$, $x \gg 0$ and $\mu \gg 0$ (reasonable for tsunamis),

$$\psi_{\text{particular}}(t,x) \simeq \left(\frac{Aq^{-3\mu-1}}{2}\right)\cdot K_q\left(\gamma\cdot q^{-\mu}[c_0 t - x]\right). \tag{3.12}$$

Finally, observe that $F_q(t,x)$ in (3.4) is q-advanced in time compared to the ground-motion profile $H_q(t,x)$. We also find that the forcing precedes the response ψ for the q-advanced models. Figure 4(a) illustrates a case where a forcing profile generates a similarly shaped tsunami in Figure 4(b).

Remark 3.2. Similar results hold for height functions $\widetilde{H}_q(t,x) \equiv \tilde{A}\cdot K_q(t/\tau)\,{}_q\mathrm{Cos}(\gamma\cdot x)$.

3.2. Numerical Solution of a q-Advanced Tsunami Wave Event

Here, we model the Japan tsunami of March 11, 2011, using (1.3), (1.4), and (1.5) with a forcing term F_q in (3.4) with environmental parameters chosen to be, in mks units,

$$\begin{aligned} g_0 &= 10\,\mathrm{ms}^{-2}, \quad H_0 = 4000\,\mathrm{m}, \quad c_0 = 200\,\mathrm{ms}^{-1},\\ \gamma &= 0.01\,\mathrm{m}^{-1}, \quad \tau = 100\,\mathrm{s}, \quad A = 6\times 10^{7}\,\mathrm{m},\end{aligned} \tag{3.13}$$

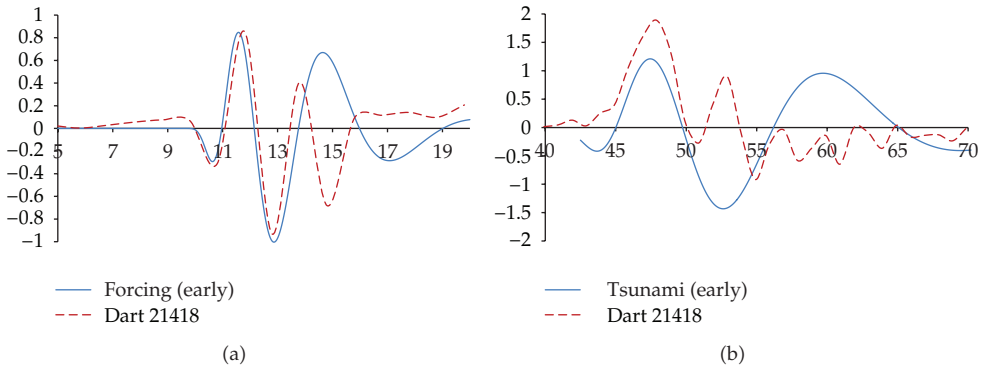

Figure 4: (a) Comparison of *forcing* from data (dashed line) and model (solid line) results in $q = 1.25$; (b) comparing *tsunami* at DART 21418 and propagation model results in $A = 6 \times 10^7$ m.

which are based on past experience [4]. The sea-depth function is chosen to be

$$H(x) = H_0, \quad \text{for } x \le 0, \qquad H(x) = H_0 \cdot \left[1 - \left(\frac{x}{5}\,\text{km}\right)^2\right], \quad \text{for } x \in (0, 5\,\text{km}), \tag{3.14}$$

which models the sea-floor near Wake Island. This is a required modification of the model used in [7]. For stability, we employ a Lax-Wendroff correction term in the numerical method. A good match with typical tsunami profiles and run-up profiles was obtained by using $q = 1.25$. In this case, $\mu \simeq 23.74$, which justifies the approximation in (3.12).

Figure 3 represents data from the Japan tsunami of March 11, 2011, at the first oceanic observation site DART 21418. This data includes a preliminary forcing profile from the (local) times 5 min to 20 min, along with the actual tsunami profile from the (local) times 42 min to 72 min.

Figure 4(a) again shows the Dart 21418 forcing profile from the times 5 min to 20 min, along with a q-advanced forcing profile as in (3.4), with A and q chosen to be $A = 6 \times 10^7$ and $q = 1.25$ to effect comparable forcing profiles.

Figure 4(b) shows the Dart 21418 actual tsunami profile from the times 42 min to 72 min along with the numerically propagated theoretical tsunami for the same time interval that was generated by (1.3) and (1.4) for the forcing F_q in (3.4) as above (with parameters $A = 6 \times 10^7$ and $q = 1.25$).

Figure 5 shows the actual tsunami profile at a later time and greater distance at oceanic observation DART 21413 from the (local) times 5 min to 65 min. Also shown for comparison is the numerically propagated theoretical tsunami for the same time interval that was generated by (1.3) and (1.4) for the forcing F_q in (3.4) with parameters $A = 6 \times 10^7$ and $q = 1.25$.

Figure 6 shows the actual run-up profile taken from the tide gauge at Wake Island at an even later time and greater distance. This is compared with our predicted run-up profile generated by (1.3) and (1.4) together with (1.5) for the forcing F_q in (3.4) with parameters $A = 6 \times 10^7$ and $q = 1.25$. The run-up data and theoretical profile have similar profiles initially, for the first few oscillations.

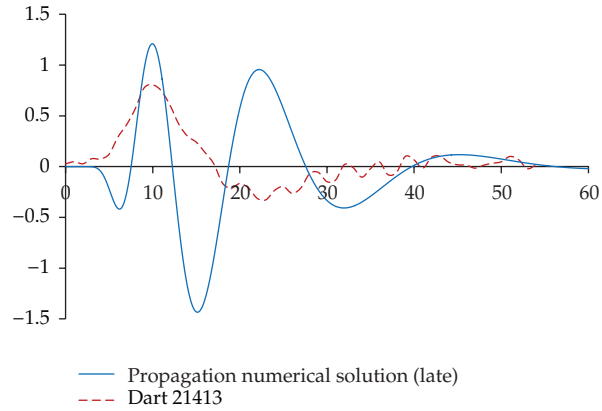

Figure 5: DART 21413: Data showing *tsunami* about 90 minutes after the earthquake and propagation model.

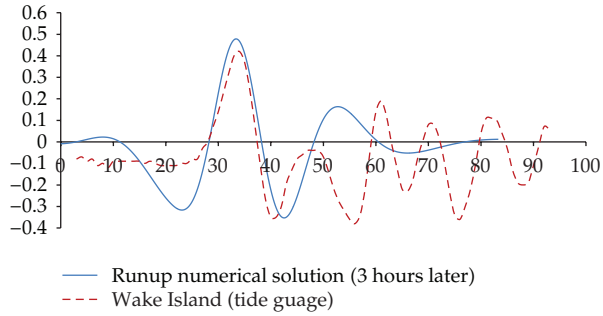

Figure 6: Wake Island: Data showing *tsunami* about 125 minutes after the earthquake and run-up model for Wake Island shoal.

4. Rogue-Wave Modeling Using Solutions of MADEs

A debate continues on the physical cause of rogue waves, [9]. One possible mechanism is a natural outcome of a constructive interference between rippling surface waves that propagate in different directions [22, page 191]. We construct a localized plane wave using a MADE-generated solution of the wave equation, for $A > 0$,

$$\Psi_q(t,x) = A \cdot {}_q\mathrm{Cos}\left(\frac{t}{\tau}\right) \cdot {}_q\mathrm{Cos}\left(\gamma \cdot x\right). \tag{4.1}$$

Substituting Ψ_q into (3.1) results in a small but persistent forcing. The model in (4.1) ignores possible translational behavior, which will be discussed at the end of this section. Here, γ and τ are parameters that satisfy $c\gamma = 1/\tau$ for a constant celerity $c > 0$. The forcing required to obtain Ψ_q from a calm distant past consists of two terms

$$F_q(t,x) = Aq\gamma^2c^2 \cdot \left[{}_q\mathrm{Cos}\left(\frac{q \cdot t}{\tau}\right) \cdot {}_q\mathrm{Cos}(\gamma \cdot x) - {}_q\mathrm{Cos}\left(\frac{t}{\tau}\right) \cdot {}_q\mathrm{Cos}(q \cdot \gamma \cdot x)\right], \tag{4.2}$$

and it is easily seen that $\|F_q\|_\infty \leq A/\tau^2$. We show that $\|F_q\|_\infty \to 0$ as $q \to 1^+$ while from (4.1) it follows that $\|\psi_q\|_\infty = A$ remains constant for all $q > 1$. This is a type of triad resonance with peak at $(t, x) = (0, 0)$. To proceed with our analysis, estimates on the differences between q-advanced functions, which are solutions of MADEs, are needed.

4.1. Analysis of Forcing Terms for ${}_q\mathrm{Cos}$ and ${}_q\mathrm{Sin}$-Type Rogue Waves

In this section, we show that small amplitude forces, over long periods of time, can naturally produce large rogue waves. This demonstrates the existence of a resonance for the system externally forced by (4.2).

Proposition 4.1. *Let $\epsilon > 0$ be given. Then there exists $Q_C^\epsilon > 1$ such that for all q with $1 < q < Q_C^\epsilon$ one has*

$$\left| {}_q\mathrm{Cos}(qt) - {}_q\mathrm{Cos}(t) \right| < \epsilon, \tag{4.3}$$

for all $t \in \mathbb{R}$; also there exists $Q_S^\epsilon > 1$ such that for all q with $1 < q < Q_S^\epsilon$ one has

$$\left| {}_q\mathrm{Sin}(qt) - {}_q\mathrm{Sin}(t) \right| < \epsilon, \tag{4.4}$$

for all $t \in \mathbb{R}$.

The proof of this result is given in the last section. It is used here to show that small amplitude forces, over long periods of time, can naturally produce rogue waves. That is, for q sufficiently near 1, we now apply Proposition 4.1 to show that for arbitrarily small forcing terms $F_q(t, x)$ there are large rogue solutions $\Psi_q(t, x)$ of the forced wave equation (4.5) (and of (4.10)).

Theorem 4.2. *Let $A, c > 0$ and define Ψ_q as in (4.1) and F_q as in (4.2). Let $\epsilon > 0$ be given, and let $q > 1$ be sufficiently close to 1. Then $\Psi_q(t, x)$ satisfies the forced wave equation*

$$\left(\partial_t^2 - c^2\partial_x^2\right)\Psi_q(t, x) = F_q(t, x), \tag{4.5}$$

where $\Psi_q(0, 0) = A$ is fixed, but $|F_q(t, x)| < \epsilon$ for all $t, x \in \mathbb{R}$.

Proof. Without loss of generality, set $\gamma = 1$ and $c = 1/\tau$. Then one has, for all $q > 1$, that

$$\begin{aligned}
\left(\partial_t^2 - c^2\partial_x^2\right)\Psi_q(t, x) &= \left(\partial_t^2 - c^2\partial_x^2\right)\left[A \cdot {}_q\mathrm{Cos}(ct) \cdot {}_q\mathrm{Cos}(x)\right] \\
&= A(-q) \cdot {}_q\mathrm{Cos}(qct)\, c^2 \cdot {}_q\mathrm{Cos}(x) \\
&\quad - c^2 A \cdot {}_q\mathrm{Cos}(ct)(-q) \cdot {}_q\mathrm{Cos}(qx) \\
&= -Aqc^2\left[{}_q\mathrm{Cos}(qct) \cdot {}_q\mathrm{Cos}(x) - {}_q\mathrm{Cos}(ct) \cdot {}_q\mathrm{Cos}(qx)\right] \\
&= F_q(t, x),
\end{aligned} \tag{4.6}$$

giving (4.5). Choose $q_0 > 1$. Now let $\tilde{\epsilon} \equiv \epsilon/[2Aq_0c^2]$, and let $Q_C^{\tilde{\epsilon}} > 1$ be chosen so that for $1 < q < Q_C^{\tilde{\epsilon}}$ one has $|{}_q\mathrm{Cos}(qx) - {}_q\mathrm{Cos}(x)| < \tilde{\epsilon}$ by Proposition 4.1. Then, for all $1 < q < \min\{Q_C^{\tilde{\epsilon}}, q_0\}$,

$$\begin{aligned}
\left|F_q(t,x)\right| &= \left|-Aqc^2\left[{}_q\mathrm{Cos}(qct)\cdot{}_q\mathrm{Cos}(x) - {}_q\mathrm{Cos}(ct)\cdot{}_q\mathrm{Cos}(x)\right]\right. \\
&\quad \left. - Aqc^2\left[{}_q\mathrm{Cos}(ct)\cdot{}_q\mathrm{Cos}(x) - {}_q\mathrm{Cos}(ct)\cdot{}_q\mathrm{Cos}(qx)\right]\right| \\
&\le Aqc^2\left|{}_q\mathrm{Cos}(x)\right|\left|\left[{}_q\mathrm{Cos}(qct) - {}_q\mathrm{Cos}(ct)\right]\right| \\
&\quad + Aqc^2\left|{}_q\mathrm{Cos}(ct)\right|\left|\left[{}_q\mathrm{Cos}(x) - {}_q\mathrm{Cos}(qx)\right]\right| \\
&\le Aqc^2 1\left|{}_q\mathrm{Cos}(qct) - {}_q\mathrm{Cos}(ct)\right| + Aqc^2 1\left|{}_q\mathrm{Cos}(qx) - {}_q\mathrm{Cos}(x)\right| \\
&\le Aqc^2\tilde{\epsilon} + Aqc^2\tilde{\epsilon} < \frac{\epsilon}{2} + \frac{\epsilon}{2} = \epsilon,
\end{aligned} \tag{4.7}$$

(4.8)

where (4.8) follows from the fact that $\|{}_q\mathrm{Cos}\|_\infty = 1$. Now, since ${}_q\mathrm{Cos}(0) = 1$, we have $\Psi_q(0,0) \equiv A\cdot{}_q\mathrm{Cos}(0)\cdot{}_q\mathrm{Cos}(0) = A$. □

Theorem 4.3. *Let $A, c > 0$. Let $\epsilon > 0$ be given, and let $q > 1$ be sufficiently close to 1. Define*

$$\begin{aligned}
\Phi_q(t,x) &\equiv A\cdot{}_q\mathrm{Sin}(ct)\cdot{}_q\mathrm{Sin}(x), \\
G_q(t,x) &\equiv -Aq^2c^2\left[{}_q\mathrm{Sin}(qct)\cdot{}_q\mathrm{Sin}(x) - {}_q\mathrm{Sin}(ct)\cdot{}_q\mathrm{Sin}(qx)\right].
\end{aligned} \tag{4.9}$$

Then $\Phi_q(t,x)$ satisfies the forced wave equation

$$\left(\partial_t^2 - c^2\partial_x^2\right)\Phi_q(t,x) = G_q(t,x), \tag{4.10}$$

where $\sup_{t,x\in\mathbb{R}}\Phi_q \approx A \gg \epsilon$, but $|G_q(t,x)| < \epsilon$ for all $t, x \in \mathbb{R}$.

Proof. From (4.9), one has for all $q > 1$ that

$$\begin{aligned}
\left(\partial_t^2 - c^2\partial_x^2\right)\Phi_q(t,x) &= \left(\partial_t^2 - c^2\partial_x^2\right)\left[A\cdot{}_q\mathrm{Sin}(ct)\cdot{}_q\mathrm{Sin}(x)\right] \\
&= A\left(-q^2\right)\cdot{}_q\mathrm{Sin}(qct)\,c^2\cdot{}_q\mathrm{Sin}(x) \\
&\quad - c^2A\cdot{}_q\mathrm{Sin}(ct)\left(-q^2\right)\cdot{}_q\mathrm{Sin}(qx) \\
&= -Aq^2c^2\left[{}_q\mathrm{Sin}(qct)\cdot{}_q\mathrm{Sin}(x) - {}_q\mathrm{Sin}(ct)\cdot{}_q\mathrm{Sin}(qx)\right] \\
&= G_q(t,x),
\end{aligned} \tag{4.11}$$

giving (4.10). Choose $q_0 > 1$. Now let $\widetilde{\epsilon} \equiv \epsilon/[2Aq_0{}^2c^2\sqrt{q_0}]$, and let $Q_S^{\widetilde{\epsilon}} > 1$ be chosen so that for $1 < q < Q_S^{\widetilde{\epsilon}}$ one has $|{}_q\mathrm{Sin}(qx) - {}_q\mathrm{Sin}(x)| < \widetilde{\epsilon}$ by Proposition 4.1. Then, for all $1 < q < \min\{Q_S^{\widetilde{\epsilon}}, q_0\}$,

$$\begin{aligned} |G_q(t,x)| &= \Big|-Aq^2c^2\Big[{}_q\mathrm{Sin}(qct)\cdot{}_q\mathrm{Sin}(x) - {}_q\mathrm{Sin}(ct)\cdot{}_q\mathrm{Sin}(x)\Big] \\ &\quad - Aq^2c^2\Big[{}_q\mathrm{Sin}(ct)\cdot{}_q\mathrm{Sin}(x) - {}_q\mathrm{Sin}(ct)\cdot{}_q\mathrm{Sin}(qx)\Big]\Big| \qquad (4.12) \\ &\le Aq^2c^2\Big|{}_q\mathrm{Sin}(x)\Big|\Big|\Big[{}_q\mathrm{Sin}(qct) - {}_q\mathrm{Sin}(ct)\Big]\Big| \\ &\quad + Aq^2c^2\Big|{}_q\mathrm{Sin}(ct)\Big|\Big|\Big[{}_q\mathrm{Sin}(x) - {}_q\mathrm{Sin}(qx)\Big]\Big| \qquad (4.13) \\ &\le Aq^2c^2\sqrt{q}\Big|{}_q\mathrm{Sin}(qct) - {}_q\mathrm{Sin}(ct)\Big| + Aq^2c^2\sqrt{q}\Big|{}_q\mathrm{Sin}(qx) - {}_q\mathrm{Sin}(x)\Big| \qquad (4.14) \\ &\le Aq^2c^2\sqrt{q}\widetilde{\epsilon} + Aqc^2\sqrt{q}\widetilde{\epsilon} < \frac{\epsilon}{2} + \frac{\epsilon}{2} = \epsilon, \qquad (4.15) \end{aligned}$$

where (4.14) follows from the fact that $\|{}_q\mathrm{Sin}\|_\infty \le \sqrt{q}$, as in [20]. Now, since $\sup {}_q\mathrm{Sin} \approx 1$ for $q > 1$ sufficiently close to 1, we have that $\sup \Phi_q \approx A$. □

4.2. Slowly Moving Rogue Waves

When a slight drift in the rogue-generating current is present, there may be a speed $v \ll c$ to the wave-height profile. A model for such a rogue can be given by

$$\psi_{q,v}(t,x) = A\cdot {}_q\mathrm{Cos}\big(\Gamma_v\cdot\gamma\cdot ct\big)\cdot {}_q\mathrm{Cos}\big(\gamma\cdot(x-vt)\big), \qquad (4.16)$$

where $\Gamma_v \equiv \sqrt{1-(v/c)^2}$. The peak of this wave still occurs at $(t,x) = (0,0)$ but moves to the right at speed v. The techniques used in the previous section show that by choice of parameters, a small amplitude forcing, over a long period, will create a moving rogue of arbitrary size.

Theorem 4.4. *Let $A, c, \gamma > 0$ and $c > v > 0$. Define $\Gamma_v \equiv \sqrt{1-(v/c)^2}$. Let $\epsilon > 0$ be given, and let $q > 1$ be sufficiently close to 1. Define the surface-height function*

$$\widetilde{\Psi}_{q,v}(t,x) \equiv A\cdot {}_q\mathrm{Cos}\big(\Gamma_v\cdot\gamma\cdot ct\big)\cdot {}_q\mathrm{Cos}\big(\gamma\cdot(x-vt)\big), \qquad (4.17)$$

and let the forcing be given by

$$\begin{aligned} \widetilde{F}_q(t,x) \equiv &-\Big(2A\gamma^2vc\Gamma_v\Big)\cdot {}_q\mathrm{Sin}\big(\Gamma_v\gamma ct\big)\ {}_q\mathrm{Sin}\big(\gamma(x-vct)\big) \\ &- A\gamma^2q\Big(c^2-v^2\Big)\cdot\Big[{}_q\mathrm{Cos}\big(q\Gamma_v\gamma ct\big)\ {}_q\mathrm{Cos}\big(\gamma(x-vt)\big) \\ &+ {}_q\mathrm{Cos}\big(\Gamma_v\gamma ct\big)\ {}_q\mathrm{Cos}\big(q\gamma(x-vt)\big)\Big]. \end{aligned} \qquad (4.18)$$

Then $\widetilde{\Psi}_{qv}(t,x)$ *satisfies the forced wave equation*

$$\left(\partial_t^2 - c^2\partial_x^2\right)\widetilde{\Psi}_{q,v}(t,x) = \widetilde{F}_q(t,x), \tag{4.19}$$

where $\widetilde{\Psi}_{q,v}(0,0) = A$ *is fixed, but* $|\widetilde{F}_q(t,x)| < \epsilon + (2Aq\Gamma_v\gamma^2 c)\cdot v$ *for all* $t,x \in \mathbb{R}$.

Proof. Applying the operator $(\partial_t^2 - c^2\partial_x^2)$ to (4.17) yields (4.19) for $\widetilde{F}_q$ in (4.18). The magnitude of the first term in (4.18) is handled as follows:

$$\begin{aligned}
&\left|\left(2A\gamma^2 vc\Gamma_v\right)\,{}_q\mathrm{Sin}(\Gamma_v\gamma ct)\;\,{}_q\mathrm{Sin}(\gamma(x-vt))\right| \\
&\quad\le \left(2A\gamma^2 vc\Gamma_v\right)\left|\,{}_q\mathrm{Sin}(\Gamma_v\gamma ct)\right|\cdot\left|\,{}_q\mathrm{Sin}(\gamma(x-vt))\right| \\
&\quad\le \left(2A\gamma^2 vc\Gamma_v\right)\sqrt{q}\sqrt{q} = \left(2A\gamma^2 qc\Gamma_v\right)\cdot v,
\end{aligned} \tag{4.20}$$

where the last inequality follows from the fact that $\|\,{}_q\mathrm{Sin}\|_\infty \le \sqrt{q}$. The remaining expressions in (4.18) are controlled by noticing that

$$\left|\,{}_q\mathrm{Cos}(q\cdot\Gamma_v\gamma ct)\cdot\,{}_q\mathrm{Cos}(\gamma(x-vt)) - {}_q\mathrm{Cos}(\Gamma_v\gamma ct)\cdot\,{}_q\mathrm{Cos}(q\cdot\gamma(x-vt))\right| \tag{4.21}$$

can be brought below ϵ for q sufficiently close to 1^+ by paralleling steps (4.7) through (4.8) in Theorem 4.2 and applying Proposition 4.1. The result is now proven. □

Remark 4.5. For v sufficiently small (as well as q sufficiently near 1^+), the term $(2Aq\Gamma_v\gamma^2 c)\cdot v$ in Theorem 4.4 is small, and one then has that $\widetilde{F}_q(t,x)$ can be made arbitrarily small compared with the rogue amplitude A, independently of $t,x \in \mathbb{R}$. For smaller values of γ, the moving rogue wave maintains a large amplitude near A for a longer period of time.

Remark 4.6. There is a corresponding theorem for the moving ${}_q\mathrm{Sin}$ rogue wave given by $\widetilde{\Phi}_{q,v}(t,x) \equiv A\cdot\,{}_q\mathrm{Sin}(\Gamma_v\gamma ct)\cdot\,{}_q\mathrm{Sin}(\gamma(x-vt))$.

Remark 4.7. Note that, as is demonstrated in Figure 7, classic rogue wave profiles emerge from smaller forcings even for q relatively far from 1.

5. Wavelet Signal Analysis, Inversion, and the Frame Operator

We now have a collection of solutions to differential equations that give the qualitative behavior of a physical phenomena. Next, to detect, analyze, store, and recover a tsunami waveform, it is common to use a wavelet analysis [25]. The process begins by identifying a discrete set of functions, called an affine frame,

$$\Lambda_\psi \equiv \left\{ \psi_{j,k}(t) \equiv \frac{q^{j/2}\psi(q^j t - kb)}{\|\psi\|}\,\middle|\, j,k \in \mathbb{Z}\right\}. \tag{5.1}$$

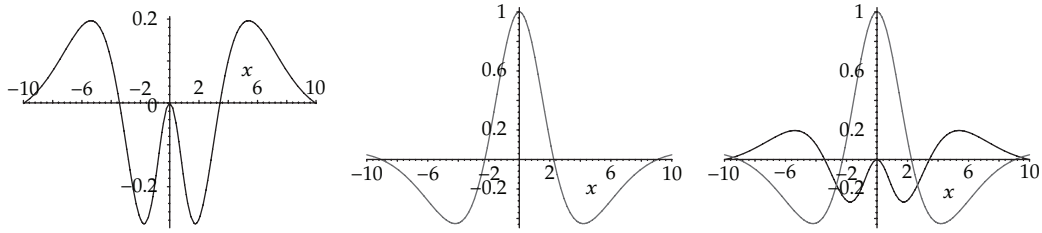

(a) (b) (c)

Figure 7: Parameters: $c = 1.0$, $\lambda = 1.0$, $\tau = q = 3/2$, and $\gamma = 1/q = 2/3$. (a) Forcing profile F_q converges toward $x = 0$ as $t \to 0^-$; (b) rogue solution Ψ_q in a neighborhood of $x = 0$ that oscillates over time; (c) forcing with $\|F_q\|_\infty \leq 1/q^2 = 4/9$ and solution with $\|\Psi_q\|_\infty = 1$.

With some effort, it can be shown that $\operatorname{span}\Lambda_\psi = \mathcal{L}^2(\mathbb{R})$, for appropriate ψ and $b > 0$ sufficiently small [26]. This leads a wavelet transform $W_\psi : \mathcal{L}^2(\mathbb{R}) \to \ell^2(\mathbb{Z}^2)$ where

$$W_\psi[f](j,k) \equiv \langle \psi_{j,k}, f \rangle = \left[\frac{q^{j/2}}{\|\psi\|} \right] \int_{\mathbb{R}} \psi\left(q^j t - kb\right) f(t)\,dt. \tag{5.2}$$

The range of W is a subspace of $\ell^2(\mathbb{Z}^2)$ and has an adjoint W^* defined to be

$$W^* : W\left[\mathcal{L}^2(\mathbb{R})\right] \subseteq \ell^2\left(\mathbb{Z}^2\right) \longrightarrow \mathcal{L}^2(\mathbb{R}), \qquad W^*\left[\{c_{j,k}\}_{\mathbb{Z}^2}\right] = \sum c_{j,k}\psi^*_{j,k}(t), \tag{5.3}$$

where $\psi^*_{j,k}$ are the elements of the dual frame to Λ_ψ. The frame operator $S \equiv W^*W : \mathcal{L}^2(\mathbb{R}) \to \mathcal{L}^2(\mathbb{R})$ is invertible for $b > 0$ sufficiently small. If Λ_ψ is an orthonormal basis for $\mathcal{L}^2(\mathbb{R})$, then one can use $\psi^*_{j,k} = \psi_{j,k}$. The wavelets K_q, ${}_q\mathrm{Cos}$, and ${}_q\mathrm{Sin}$ generate frames whose inner product structures are nearly orthogonal [20]. Consequently, as will be shown below, a reasonable analysis of the different waveforms is obtained without computing the dual to Λ_ψ.

The results of a signal analysis and synthesis, briefly presented here, consist of (1) choosing 256 equallyspaced points from the data, (2) computing the inner products with elements of Λ_ψ, (3) sorting and identifying inner products with the largest magnitudes, (4) reconstructing the wavelet-based waveform, (5) normalizing in $\mathcal{L}^2$, and (6) computing the normalized RMS error.

By [19], the sizes chosen for the parameters are $q = 1.5$ and $b \sim 2$, with slight adjustments being made to improve the result. The reconstructed signal has an amplitude about $b/(2q)$ of the size of the data profile. The need for this scaling was explained in [20] and is due to the fact that the $\mathcal{L}^2$ operator norm of S^{-1} is estimated to be $b/(2q)$.

5.1. Tsunami Wavelet Analysis

On March 11, 2011, an earthquake of magnitude 9.0 occurred off the coast of Japan causing a tsunami no less than 10 m high. Surface wave levels were detected by buoys operated by

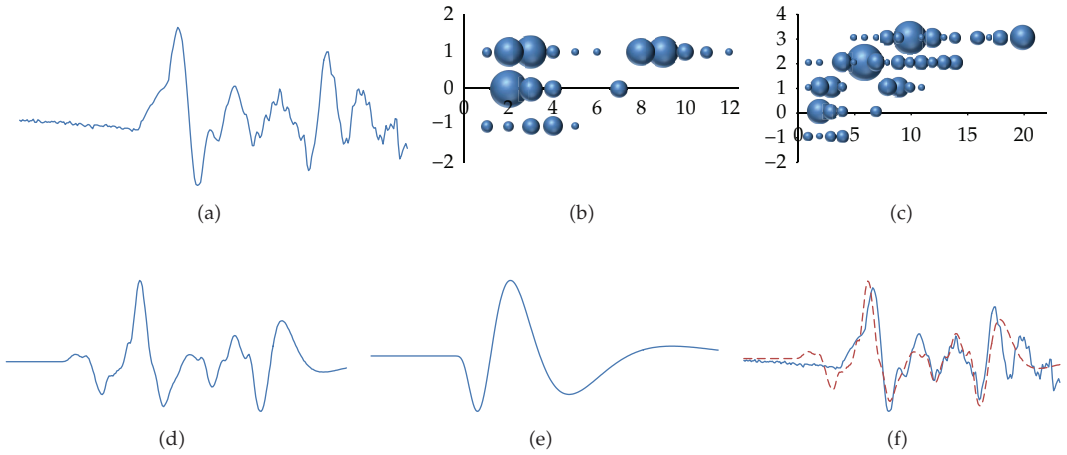

Figure 8: (a) Tsunami 46411 from DART, March 2011; (b) relative magnitude of coefficients for 3 scales $\{q^{-1}, 1, q\}$ for $q = 1.5$; (c) relative magnitude of coefficients for 5 scales $\{q^j\}_{j=-1}^{3}$; (d) $K_q(t)$ wavelet approximation with 20 largest coefficients; (e) largest magnitude of K_q ($q = 1.5$, scale $= q^0 = 1$, shift $= 2 \cdot b = 3.9$); (f) comparison between DART data and K_q wavelet reconstruction.

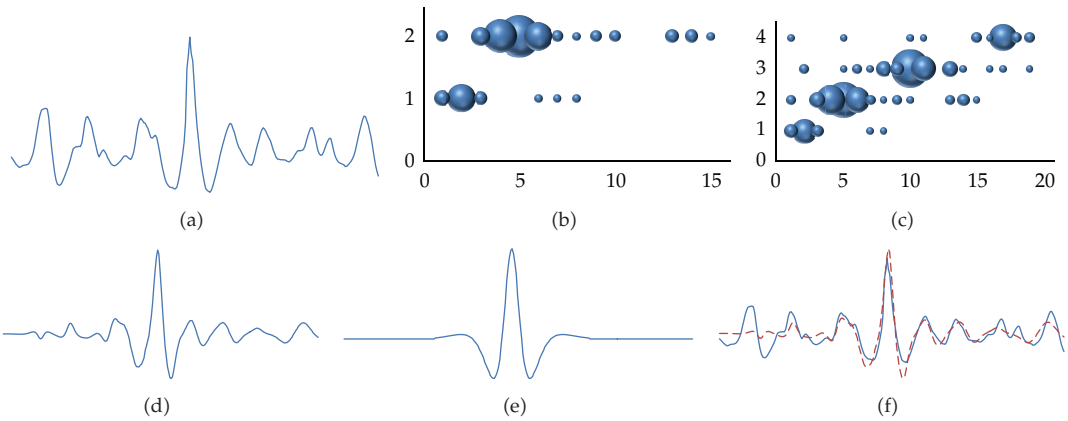

Figure 9: (a) Rogue 1520 from Draupner, January 1995; (b) relative magnitude of coefficients for 3 scales $\{1, q, q^2\}$ for $q = 1.5$; (c) relative magnitude of coefficients for 5 scales $\{q^j\}_{j=0}^{4}$; (d) ${}_q\mathrm{Cos}$ wavelet approximation using largest 30 coefficients; (e) largest magnitude of ${}_q\mathrm{Cos}$ ($q = 1.5$, scale $= q^2$, shift $= 5 \cdot b = 12.2$); (f) comparison between Draupner data and ${}_q\mathrm{Cos}$ wavelet reconstruction.

DART. To detect, analyze, store, and recover a tsunami waveform, we choose the wavelet frame

$$\Lambda_{K_q} = \left\{ \sqrt{\frac{q^j}{C_K}} \cdot K_q\left(q^j t - kb\right) \middle| j, k \in \mathbb{Z} \right\}, \quad C_K \equiv \int_0^\infty K_q^2(t)\,dt, \tag{5.4}$$

with $q = 1.5$ and $b = 1.95$. Then the application of W_{K_q} on tsunami data gives coefficients $\{c_{j,k}\}$ which can be plotted in a k versus j diagram. The largest values of $|c_{j,k}|$ indicate position

(due to k) and narrowness (due to j). Only the largest 20 coefficients in magnitude, for the ranges $-1 \le j \le 3$ and $1 \le k \le 10$, were used to obtain the fit on the bottom right of Figure 8. The normalized-RMS error

$$\mathrm{NRMSE} \equiv \frac{1}{\max\left(y_i^{\mathrm{wavelet}}\right) - \min\left(y_i^{\mathrm{wavelet}}\right)} \cdot \left(\frac{1}{N}\sum_{i=1}^{N}\left(y_i^{\mathrm{data}} - y_i^{\mathrm{wavelet}}\right)^2\right)^{1/2} \tag{5.5}$$

was computed to be NRMSE = 16%. The bubble plots of the relative sizes of the coefficients are shown with the discrete *time translation* variable k displayed horizontally, and the discrete *frequency exponent* j displayed vertically.

5.2. Rogue Wavelet Analysis

On January 1, 1995, a rogue wave was detected on the Draupner platform in the North Sea. Surface wave heights were recorded using a laser-detection method [10]. Here we use the wavelet frame

$$\Lambda_q\mathrm{Cos} = \left\{\sqrt{\frac{q^j}{C_C}} \cdot {}_q\mathrm{Cos}\left(q^j t - kb\right) \mid \; j,k \in \mathbb{Z}\right\}, \quad C_C \equiv \int_0^\infty {}_q\mathrm{Cos}^2(t)\,dt, \tag{5.6}$$

with $q = 1.5$ and $b = 2.44$. Here, we used 30 coefficients, for the ranges $1 \le j \le 4$ and $1 \le k \le 10$, to obtain the fit on the bottom right. The normalized RMS error is 18%. See Figure 9 for the results of this analysis.

6. Estimates for $|{}_q\mathrm{Cos}(qt) - {}_q\mathrm{Cos}(t)|$ and $|{}_q\mathrm{Sin}(qt) - {}_q\mathrm{Sin}(t)|$

In this section, the estimates for the differences of q-advanced trigonometric functions are proven. First we record useful Fourier transform expressions. From (2.3) we have the Fourier transforms of ${}_q\mathrm{Cos}(t)$, ${}_q\mathrm{Cos}(qt)$, ${}_q\mathrm{Sin}(t)$, and ${}_q\mathrm{Sin}(qt)$, respectively, are given by

$$\mathcal{F}\left[{}_q\mathrm{Cos}(t)\right](\omega) = \frac{2\left(\mu_{q^2}\right)^3 N_q}{\sqrt{2\pi}} \frac{1}{\theta\left(q^2;\omega^2\right)}, \tag{6.1}$$

$$\mathcal{F}\left[{}_q\mathrm{Cos}(qt)\right](\omega) = \frac{1}{q}\frac{2\left(\mu_{q^2}\right)^3 N_q}{\sqrt{2\pi}} \frac{1}{\theta\left(q^2;\left(q^2\right)^{-1}\omega^2\right)} = \frac{\omega^2}{q}\mathcal{F}\left[{}_q\mathrm{Cos}(t)\right](\omega), \tag{6.2}$$

$$\mathcal{F}\left[{}_q\mathrm{Sin}(t)\right](\omega) = \frac{2\left(\mu_{q^2}\right)^3 N_q}{\sqrt{2\pi}} \frac{(-i\omega)}{\theta\left(q^2;\omega^2\right)}, \tag{6.3}$$

$$\mathcal{F}\left[{}_q\mathrm{Sin}(qt)\right](\omega) = \frac{1}{q}\frac{2\left(\mu_{q^2}\right)^3 N_q}{\sqrt{2\pi}} \frac{(-i\omega/q)}{\theta\left(q^2;\left(q^2\right)^{-1}\omega^2\right)} = \frac{\omega^2}{q^2}\mathcal{F}\left[{}_q\mathrm{Sin}(t)\right](\omega), \tag{6.4}$$

where the algebraic identity $\theta(q^2;(q^2)^n\omega^2) = (q^2)^{n(n+1)/2}(\omega^2)^n\theta(q^2;\omega^2)$, that follows from (2.6), was used to obtain (6.2) and (6.4). Further details are presented in [21].

Proof of Proposition 4.1. We first prove the estimate for the differences involving ${}_q\mathrm{Cos}$. From (6.1) and (6.2), one has

$$\begin{aligned}
\left|{}_q\mathrm{Cos}(qt) - {}_q\mathrm{Cos}(t)\right| &= \left|\mathcal{F}^{-1}\left(\mathcal{F}\left[{}_q\mathrm{Cos}(qt)\right]\right) - \mathcal{F}^{-1}\left(\mathcal{F}\left[{}_q\mathrm{Cos}(t)\right]\right)\right| \\
&= \frac{1}{\sqrt{2\pi}}\left|\int_{\mathbb{R}} e^{i\omega t}\left\{\frac{1}{q}\frac{2(\mu_{q^2})^3N_q}{\sqrt{2\pi}}\frac{\omega^2}{\theta(q^2;\omega^2)}\right.\right. \\
&\qquad\left.\left. -\frac{2(\mu_{q^2})^3N_q}{\sqrt{2\pi}}\frac{1}{\theta(q^2;\omega^2)}\right\}d\omega\right| \qquad (6.5) \\
&\le \frac{1}{\sqrt{2\pi}}\frac{1}{q}\frac{2(\mu_{q^2})^3N_q}{\sqrt{2\pi}}\int_{\mathbb{R}}\frac{|\omega^2-q|}{\theta(q^2;\omega^2)}d\omega = \frac{2(\mu_{q^2})^3N_q}{2\pi q}2\int_0^\infty\frac{|\omega^2-q|}{\theta(q^2;\omega^2)}d\omega, \qquad (6.6) \\
&= \frac{2}{\pi q}(\mu_{q^2})^3N_q\left[\int_0^1\frac{|\omega^2-q|}{\theta(q^2;\omega^2)}d\omega + \int_1^\infty\frac{|\omega^2-q|}{\theta(q^2;\omega^2)}d\omega\right], \qquad (6.7)
\end{aligned}$$

where the triangle inequality gives the inequality in (6.6), and the evenness of $|\omega^2 - q|/\theta(q^2;\omega^2)$ allows for reduction to integration over $[0,\infty)$ in (6.6).

The change of variables $\omega = 1/u$ is made on the first integral in (6.7), and the algebraic identity $\theta(q^2;u^{-2}) = u^{-2}\theta(q^2;u^2)$ is used to obtain

$$\int_0^1\frac{|\omega^2-q|}{\theta(q^2;\omega^2)}d\omega = \int_\infty^1\frac{|u^{-2}-q|}{\theta(q^2;u^{-2})}\left(-u^{-2}\right)du = \int_1^\infty\frac{|u^{-2}-q|}{\theta(q^2;u^2)}du. \qquad (6.8)$$

Now (6.8) is used to reexpress the bound (6.7) as

$$\left|{}_q\mathrm{Cos}(qt) - {}_q\mathrm{Cos}(t)\right| \le \frac{2}{\pi q}(\mu_{q^2})^3N_q\int_1^\infty\frac{|\omega^{-2}-q| + |\omega^2-q|}{\theta(q^2;\omega^2)}d\omega. \qquad (6.9)$$

From (2.9), we have that

$$\begin{aligned}
\frac{1}{\theta(q^2;\omega^2)} &\le \left[q^{1/4}|\omega|e^{(\ln(|\omega|))^2/\ln(q)}\left\{\sqrt{\frac{\pi}{\ln(q)}} - 1\right\}\right]^{-1} \\
&= \ln(q)\left[\frac{1}{\sqrt{\ln(q)}}\frac{q^{-1/4}|\omega|^{-1}e^{-(\ln(|\omega|))^2/\ln(q)}}{\left\{\sqrt{\pi} - \sqrt{\ln(q)}\right\}}\right], \qquad (6.10)
\end{aligned}$$

for $1 < q < e^{\pi}$. Deploying the bound (6.10) within the integral in the bound (6.9) gives

$$\left| {}_q\mathrm{Cos}(qt) - {}_q\mathrm{Cos}(t) \right| \leq F(q) \left[\frac{1}{\sqrt{\ln(q)}} \int_1^{\infty} \frac{\{ |\omega^{-2} - q| + |\omega^2 - q| \} \omega^{-1}}{e^{(\ln \omega)^2 / \ln(q)}} d\omega \right], \tag{6.11}$$

where

$$F(q) \equiv \frac{2 \ln(q) (\mu_{q^2})^3 N_q}{\pi q^{5/4}} \frac{1}{\sqrt{\pi} - \sqrt{\ln(q)}}. \tag{6.12}$$

It follows from [21] that

$$\lim_{q \to 1^+} \left[\ln(q) (\mu_{q^2})^3 N_q \right] = \frac{\pi}{2} \Longrightarrow \lim_{q \to 1^+} F(q) = \frac{1}{\sqrt{\pi}}. \tag{6.13}$$

We now show that $| {}_q\mathrm{Cos}(qt) - {}_q\mathrm{Cos}(t) |$ can be made arbitrarily small, independently of t, for all $q > 1$ sufficiently close to 1^+. In light of (6.13), this is accomplished by first showing the corresponding statement holds for the bracketed expression in (6.11).

Let $\alpha > 0$ be arbitrary, with α to be specified later. The integral in ω over the interval $[1, \infty)$ in (6.11) is now subdivided into two integrals, the first over $[1, e^{\alpha\sqrt{\ln(q)}}]$ and the second over $[e^{\alpha\sqrt{\ln(q)}}, \infty)$. First, considering ω restricted to the interval $[1, e^{\alpha\sqrt{\ln(q)}}]$, one has that

$$\begin{aligned} &\frac{1}{\sqrt{\ln(q)}} \int_1^{e^{\alpha\sqrt{\ln(q)}}} \frac{\{ |\omega^{-2} - q| + |\omega^2 - q| \} \omega^{-1}}{e^{(\ln \omega)^2 / \ln(q)}} d\omega \\ &\quad \leq \frac{1}{\sqrt{\ln(q)}} \int_1^{e^{\alpha\sqrt{\ln(q)}}} \frac{\{ |\omega^{-2} - q| \omega^2 + |\omega^2 - q| \} \omega^{-1}}{e^{(\ln \omega)^2 / \ln(q)}} d\omega \\ &\quad = \frac{1}{\sqrt{\ln(q)}} \int_1^{e^{\alpha\sqrt{\ln(q)}}} \frac{\{ |\omega^{-1} - q\omega| + |\omega - q\omega^{-1}| \}}{e^{(\ln \omega)^2 / \ln(q)}} d\omega. \end{aligned} \tag{6.14}$$

Now the function $|\omega^{-1} - q\omega|$ assumes its maximum value on $[1, e^{\alpha\sqrt{\ln(q)}}]$ at the right endpoint $e^{\alpha\sqrt{\ln(q)}}$. In addition, for all q sufficiently close to 1, the function $|\omega - q\omega^{-1}|$ assumes its maximum value on $[1, e^{\alpha\sqrt{\ln(q)}}]$ at the right endpoint $e^{\alpha\sqrt{\ln(q)}}$. The latter statement follows since $g(\omega) = \omega - q\omega^{-1}$ is increasing, and one needs only to compare endpoints $|g(1)| = q - 1$ and $|g(e^{\alpha\sqrt{\ln(q)}})| = e^{\alpha\sqrt{\ln(q)}} - qe^{-\alpha\sqrt{\ln(q)}}$ to determine the larger value. An application of L'Hopital's

rule gives that $\lim_{q\to 1^+}|g(e^{\alpha\sqrt{\ln(q)}})|/|g(1)| = \infty$. Thus, for q near 1, on the interval $[1, e^{\alpha\sqrt{\ln(q)}}]$, one has

$$\begin{aligned}\left\{\left|\omega^{-1}-q\omega\right|+\left|\omega-q\omega^{-1}\right|\right\} &\le \left|e^{-\alpha\sqrt{\ln(q)}}-qe^{\alpha\sqrt{\ln(q)}}\right|+\left|e^{\alpha\sqrt{\ln(q)}}-qe^{-\alpha\sqrt{\ln(q)}}\right| \\ &= qe^{\alpha\sqrt{\ln(q)}}-e^{-\alpha\sqrt{\ln(q)}}+e^{\alpha\sqrt{\ln(q)}}-qe^{-\alpha\sqrt{\ln(q)}} \\ &= (q+1)\left(e^{\alpha\sqrt{\ln(q)}}-e^{-\alpha\sqrt{\ln(q)}}\right).\end{aligned} \tag{6.15}$$

Thus, we bound the integral in (6.14) by the length of the interval times the bound (6.15) on the numerator. This gives

$$\begin{aligned}&\frac{1}{\sqrt{\ln(q)}}\int_1^{e^{\alpha\sqrt{\ln(q)}}}\frac{\left\{\left|\omega^{-1}-q\omega\right|+\left|\omega-q\omega^{-1}\right|\right\}}{e^{(\ln\omega)^2/\ln(q)}}d\omega \\ &\quad\le \frac{1}{\sqrt{\ln(q)}}\int_1^{e^{\alpha\sqrt{\ln(q)}}}(q+1)\left(e^{\alpha\sqrt{\ln(q)}}-e^{-\alpha\sqrt{\ln(q)}}\right)d\omega \\ &\quad\le \frac{1}{\sqrt{\ln(q)}}(q+1)\left(e^{\alpha\sqrt{\ln(q)}}-e^{-\alpha\sqrt{\ln(q)}}\right)\left(e^{\alpha\sqrt{\ln(q)}}-1\right).\end{aligned} \tag{6.16}$$

An application of L'Hopital's rule gives that

$$\lim_{q\to 1^+}\frac{\left(e^{\alpha\sqrt{\ln(q)}}-e^{-\alpha\sqrt{\ln(q)}}\right)}{\sqrt{\ln(q)}} = 2\alpha, \tag{6.17}$$

which implies that in (6.16) we have

$$\lim_{q\to 1^+}\left[(q+1)\frac{\left(e^{\alpha\sqrt{\ln(q)}}-e^{-\alpha\sqrt{\ln(q)}}\right)}{\sqrt{\ln(q)}}\left(e^{\alpha\sqrt{\ln(q)}}-1\right)\right] = 2\cdot 2\alpha\cdot 0 = 0. \tag{6.18}$$

Combining (6.18) with (6.16) and (6.14) gives that

$$\lim_{q\to 1^+}\left[\frac{1}{\sqrt{\ln(q)}}\int_1^{e^{\alpha\sqrt{\ln(q)}}}\frac{\left\{\left|\omega^{-2}-q\right|+\left|\omega^2-q\right|\right\}\omega^{-1}}{e^{(\ln\omega)^2/\ln(q)}}d\omega\right] = 0. \tag{6.19}$$

We next estimate the portion of the integral in (6.11) over the interval $[e^{\alpha\sqrt{\ln(q)}}, \infty)$.

$$\begin{aligned}
&\frac{1}{\sqrt{\ln(q)}} \int_{e^{\alpha\sqrt{\ln(q)}}}^{\infty} \frac{\left\{\left|\omega^{-2}-q\right| + \left|\omega^{2}-q\right|\right\}\omega^{-1}}{e^{(\ln\omega)^2/\ln(q)}} d\omega \\
&\quad = \frac{1}{\sqrt{\ln(q)}} \int_{e^{\alpha\sqrt{\ln(q)}}}^{\infty} \frac{\left\{\left|\omega^{-3}-q\omega^{-1}\right| + \left|\omega - q\omega^{-1}\right|\right\}}{e^{(\ln\omega)^2/\ln(q)}} d\omega \\
&\quad \leq \frac{1}{\sqrt{\ln(q)}} \int_{e^{\alpha\sqrt{\ln(q)}}}^{\infty} \frac{\left\{\omega^{-3} + 2q\omega^{-1} + \omega\right\}}{e^{(\ln\omega)^2/\ln(q)}} d\omega,
\end{aligned} \tag{6.20}$$

by bounding the integrals of the summands in (6.20). For each exponent $k \in \mathbb{Z}$ one has

$$\begin{aligned}
\frac{1}{\sqrt{\ln(q)}} \int_{e^{\alpha\sqrt{\ln(q)}}}^{\infty} \frac{\omega^k}{e^{(\ln\omega)^2/\ln(q)}} d\omega &= \frac{1}{\sqrt{\ln(q)}} \int_{e^{\alpha\sqrt{\ln(q)}}}^{\infty} e^{k\ln\omega} e^{-(\ln\omega)^2/\ln(q)} d\omega \\
&= \frac{q^{k^2/4}}{\sqrt{\ln(q)}} \int_{e^{\alpha\sqrt{\ln(q)}}}^{\infty} e^{-(1/\ln(q))[\ln\omega - k\ln(q)/2]^2} d\omega,
\end{aligned} \tag{6.21}$$

where a completion of squares gives (6.21). We use the following estimate from [21]

$$\int_{C}^{\infty} e^{-A[\ln\omega + B]^2} d\omega \leq \frac{\sqrt{\pi}}{2} \frac{e^{1/(4A)-B}}{\sqrt{A}} e^{-A[\ln(C)+B-1/(2A)]^2}, \tag{6.22}$$

which is applied to (6.21) with $A = 1/\ln(q)$, $B = -k\ln(q)/2$, and $C = e^{\alpha\sqrt{\ln(q)}}$ to obtain

$$\begin{aligned}
&\frac{q^{k^2/4}}{\sqrt{\ln(q)}} \int_{e^{\alpha\sqrt{\ln(q)}}}^{\infty} e^{-(1/\ln(q))[\ln\omega - k\ln(q)/2]^2} d\omega \\
&\quad \leq \frac{q^{k^2/4}}{\sqrt{\ln(q)}} \frac{\sqrt{\pi}}{2} \frac{e^{\ln(q)/4 + k\ln(q)/2}}{\sqrt{1/\ln(q)}} e^{-(1/\ln(q))[\ln(e^{\alpha\sqrt{\ln(q)}}) - k\ln(q)/2 - \ln(q)/2]^2} \\
&\quad = q^{(k+1)^2/4} \frac{\sqrt{\pi}}{2} e^{-(1/\ln(q))[\alpha\sqrt{\ln(q)} - (k+1)\ln(q)/2]^2} \\
&\quad = q^{(k+1)^2/4} \frac{\sqrt{\pi}}{2} e^{-\alpha^2 + \alpha(k+1)\sqrt{\ln(q)} - (k+1)^2\ln(q)/4} \\
&\quad = \frac{\sqrt{\pi}}{2} e^{-\alpha^2} e^{\alpha(k+1)\sqrt{\ln(q)}}.
\end{aligned} \tag{6.23}$$

Combining (6.21) and (6.23) gives that, for each $k \in \mathbb{Z}$,

$$\frac{1}{\sqrt{\ln(q)}} \int_{e^{\alpha\sqrt{\ln(q)}}}^{\infty} \frac{\omega^k}{e^{(\ln\omega)^2/\ln(q)}} d\omega \leq \frac{\sqrt{\pi}}{2} e^{-\alpha^2} e^{\alpha(k+1)\sqrt{\ln(q)}}. \tag{6.24}$$

Revisiting (6.20) and applying (6.24) now gives

$$\frac{1}{\sqrt{\ln(q)}} \int_{e^{\alpha\sqrt{\ln(q)}}}^{\infty} \frac{\{|\omega^{-2} - q| + |\omega^2 - q|\}\omega^{-1}}{e^{(\ln\omega)^2/\ln(q)}} d\omega \tag{6.25}$$

$$\leq \frac{1}{\sqrt{\ln(q)}} \int_{e^{\alpha\sqrt{\ln(q)}}}^{\infty} \frac{\{\omega^{-3} + 2q\omega^{-1} + \omega\}}{e^{(\ln\omega)^2/\ln(q)}} d\omega \tag{6.26}$$

$$\leq \frac{\sqrt{\pi}}{2} e^{-\alpha^2} \left[e^{\alpha(-2)\sqrt{\ln(q)}} + 2q e^{\alpha(0)\sqrt{\ln(q)}} + e^{\alpha(2)\sqrt{\ln(q)}} \right].$$

Since the expression in (6.26) approaches $2\sqrt{\pi}e^{-\alpha^2}$ as $q \to 1^+$, by choosing α sufficiently large one can make (6.26), and hence (6.25), arbitrarily small for q sufficiently close to 1.

Now, let $\epsilon > 0$ be given. By (6.11) we have for all $\alpha > 0$

$$\begin{aligned} \left| {}_q\mathrm{Cos}(qt) - {}_q\mathrm{Cos}(t) \right| \leq {} & F(q) \left[\frac{1}{\sqrt{\ln(q)}} \int_1^{e^{\alpha\sqrt{\ln(q)}}} \frac{\{|\omega^{-2} - q| + |\omega^2 - q|\}\omega^{-1}}{e^{(\ln\omega)^2/\ln(q)}} d\omega \right] \\ & + F(q) \left[\frac{1}{\sqrt{\ln(q)}} \int_{e^{\alpha\sqrt{\ln(q)}}}^{\infty} \frac{\{|\omega^{-2} - q| + |\omega^2 - q|\}\omega^{-1}}{e^{(\ln\omega)^2/\ln(q)}} d\omega \right]. \end{aligned} \tag{6.27}$$

One has from (6.13)

$$\lim_{q \to 1^+} F(q) \frac{\sqrt{\pi}}{2} e^{-\alpha^2} \left[e^{\alpha(-2)\sqrt{\ln(q)}} + 2q e^{\alpha(0)\sqrt{\ln(q)}} + e^{\alpha(2)\sqrt{\ln(q)}} \right] = 2e^{-\alpha^2}. \tag{6.28}$$

Choose $\tilde{A} > 2$ and then fix $\alpha > 0$ such that $\tilde{A}e^{-\alpha^2} < \epsilon/2$. By (6.26) and (6.28), there exists $q_1 = q_1(\tilde{A}, \alpha, \epsilon)$ such that for all $1 < q < q_1$ one has

$$\begin{aligned} 0 < {} & F(q) \left[\frac{1}{\sqrt{\ln(q)}} \int_{e^{\alpha\sqrt{\ln(q)}}}^{\infty} \frac{\{|\omega^{-2} - q| + |\omega^2 - q|\}\omega^{-1}}{e^{(\ln\omega)^2/\ln(q)}} d\omega \right] \\ & \leq F(q) \frac{\sqrt{\pi}}{2} e^{-\alpha^2} \left[e^{\alpha(-2)\sqrt{\ln(q)}} + 2q e^{\alpha(0)\sqrt{\ln(q)}} + e^{\alpha(2)\sqrt{\ln(q)}} \right] < \tilde{A}e^{-\alpha^2} < \frac{\epsilon}{2}. \end{aligned} \tag{6.29}$$

For this value of α, by virtue of (6.19), one has

$$\lim_{q\to 1^+} F(q)\left[\frac{1}{\sqrt{\ln(q)}}\int_1^{e^{\alpha\sqrt{\ln(q)}}} \frac{\{|\omega^{-2}-q|+|\omega^2-q|\}\omega^{-1}}{e^{(\ln\omega)^2/\ln(q)}}d\omega\right] = \frac{1}{\sqrt{\pi}}\cdot 0 = 0, \tag{6.30}$$

which in turn says that there is a $q_2 = q_2(\alpha,\epsilon)$ such that for all $1 < q < q_2$ one has

$$0 < F(q)\left[\frac{1}{\sqrt{\ln(q)}}\int_1^{e^{\alpha\sqrt{\ln(q)}}} \frac{\{|\omega^{-2}-q|+|\omega^2-q|\}\omega^{-1}}{e^{(\ln\omega)^2/\ln(q)}}d\omega\right] < \frac{\epsilon}{2}. \tag{6.31}$$

Thus, for $Q_C^\epsilon = Q(\tilde{A},\alpha,\epsilon) = \min\{q_1,q_2\}$, and for all $1 < q < Q_C^\epsilon$, applying (6.31) and (6.29) to (6.27) yields

$$\left|{}_q\mathrm{Cos}(qt) - {}_q\mathrm{Cos}(t)\right| < \frac{\epsilon}{2}+\frac{\epsilon}{2} < \epsilon, \tag{6.32}$$

independently of $t\in\mathbb{R}$. The proposition is now proven for ${}_q\mathrm{Cos}$.

The proof for ${}_q\mathrm{Sin}$ parallels the above argument for ${}_q\mathrm{Cos}$, so we only outline it here, indicating points of slight differences. From (6.3) and (6.4), the analogue of (6.6) becomes (6.33) below

$$\begin{aligned}\left|{}_q\mathrm{Sin}(qt) - {}_q\mathrm{Sin}(t)\right| &= \left|\mathcal{F}^{-1}\left(\mathcal{F}\left[{}_q\mathrm{Sin}(qt)\right]\right) - \mathcal{F}^{-1}\left(\mathcal{F}\left[{}_q\mathrm{Sin}(t)\right]\right)\right| \\ &\le \frac{1}{\sqrt{2\pi}}\frac{1}{q^2}\frac{2(\mu_{q^2})^3 N_q}{\sqrt{2\pi}}\int_{\mathbb{R}}\frac{|\omega^3-q^2\omega|}{\theta(q^2;\omega^2)}d\omega \qquad (6.33)\\ &= \frac{2(\mu_{q^2})^3 N_q}{\pi q^2}\int_0^\infty \frac{|\omega^3-q^2\omega|}{\theta(q^2;\omega^2)}d\omega, \\ &= \frac{2}{\pi q^2}(\mu_{q^2})^3 N_q\int_1^\infty \frac{|\omega^{-3}-q^2\omega^{-1}|+|\omega^3-q^2\omega|}{\theta(q^2;\omega^2)}d\omega, \qquad (6.34)\end{aligned}$$

where a reciprocation change of variables on the integral on $[0,1]$ converts to an integral on $[1,\infty)$, yielding (6.34) as the analogue of (6.9). Deploying the bound (6.10) to (6.34) now gives

$$\left|{}_q\mathrm{Sin}(qt) - {}_q\mathrm{Sin}(t)\right| \le \frac{F(q)}{q}\left[\frac{1}{\sqrt{\ln(q)}}\int_1^\infty \frac{\{|\omega^{-4}-q^2\omega^{-2}|+|\omega^2-q^2|\}}{e^{(\ln\omega)^2/\ln(q)}}d\omega\right], \tag{6.35}$$

with $F(q)$ defined in (6.12). For the integral in ω in (6.35) over the interval $[e^{\alpha\sqrt{\ln(q)}},\infty)$, an application of (6.24) in conjunction with the triangle inequality lets us proceed directly to an

analogue of (6.26), with key factor $e^{-\alpha^2}$ still intact and the remaining factor approaching a constant as $q \to 1^+$. On the other hand, the integral over the interval $[1, e^{\alpha\sqrt{\ln(q)}}]$ in (6.35) proceeds as follows. One has

$$\begin{aligned}
&\left[\frac{1}{\sqrt{\ln(q)}}\int_1^{e^{\alpha\sqrt{\ln(q)}}} \frac{\left\{\left|\omega^{-4}-q^2\omega^{-2}\right|+\left|\omega^2-q^2\right|\right\}}{e^{(\ln\omega)^2/\ln(q)}}d\omega\right] \\
&\quad\le \left[\frac{1}{\sqrt{\ln(q)}}\int_1^{e^{\alpha\sqrt{\ln(q)}}} \left\{\left|\omega^{-4}-q^2\omega^{-2}\right|\omega^2+\left|\omega^2-q^2\right|\right\}d\omega\right] \\
&\quad= \left[\frac{1}{\sqrt{\ln(q)}}\int_1^{e^{\alpha\sqrt{\ln(q)}}} \left\{\left|\omega^{-2}-q^2\right|+\left|\omega^2-q^2\right|\right\}d\omega\right] \qquad (6.36) \\
&\quad\le \frac{1}{\sqrt{\ln(q)}}\left\{\left|e^{-2\alpha\sqrt{\ln(q)}}-q^2\right|+\left|e^{2\alpha\sqrt{\ln(q)}}-q^2\right|\right\}\left[e^{\alpha\sqrt{\ln(q)}}-1\right] \\
&\quad= \frac{1}{\sqrt{\ln(q)}}\left\{-e^{-2\alpha\sqrt{\ln(q)}}+e^{2\alpha\sqrt{\ln(q)}}\right\}\left[e^{\alpha\sqrt{\ln(q)}}-1\right], \qquad (6.37)
\end{aligned}$$

where (6.36) and (6.37) hold for q sufficiently near 1^+. Since $\lim_{x\to 0}[(-e^{-2\alpha x}+e^{2\alpha x})/x] = 4\alpha$, we have the limit as $q \to 1^+$ of expression (6.37) is 0. The remainder of the proof is now entirely parallel to that of the ${}_q\mathrm{Cos}$ case. □

Acknowledgments

The rogue data from the Draupner platform was graciously supplied by Dr. Sverre Haver from Statoil, Norway. The tsunami data came from DART buoys and was graciously provided by Dr. George Mongov at NOAA. The DART data is kept at the National Geophysical Data Center/World Data Center (NGDC/WDC) Historical Tsunami Database, Boulder, CO, USA. Figure 1 profile was permitted for our use here by Dr. Benny Grosen. The authors are grateful for their assistance. Finally, they thank the referee for suggestions for improving the paper.

References

[1] G. D. Fraser, J. P. Eaton, and C. K. Wentworth, "The tsunami of March 9, 1957, on the island of Hawaii," *Bulletin of the Seismological Society of America*, vol. 49, no. 1, pp. 79–90, 1959.

[2] E. L. Geist, P. J. Lynett, and J. D. Chaytor, "Hydrodynamic modeling of tsunamis from the Currituck landslide," *Marine Geology*, vol. 264, no. 1-2, pp. 41–52, 2009.

[3] S. N. Ward, "Relationships of tsunami generation and an earthquake source," *Journal of Physics of the Earth*, vol. 28, no. 5, pp. 441–474, 1980.

[4] X. Zhao, B. Wang, and H. Liu, "Propagation and runup of tsunami waves with Boussinesq model," in *Proceedings of the 32nd International Conference on Coastal Engineering*, 2010.

[5] S. Tadepalli and C. E. Synolakis, "The run-up of N-waves on sloping beaches," *Proceedings of the Royal Society A*, vol. 445, no. 1923, pp. 99–112, 1994.

[6] D. Dunbar, P. LeBlond, and T. S. Murty, "Evaluation of tsunami amplitudes for the Pacific Coast of Canada," *Progress in Oceanography*, vol. 26, no. 2, pp. 115–177, 1991.

[7] E. van Groesen, D. Adytia, and Antodnowati, "Near-coast tsunami waveguiding: phenomenon and simulations," *Natural Hazards and Earth System Sciences*, vol. 8, no. 2, pp. 175–185, 2008.

[8] S. Tadepalli and C. E. Synolakis, "Model for the leading waves of tsunamis," *Physical Review Letters*, vol. 77, no. 10, pp. 2141–2144, 1996.

[9] T. A. A. Adcock, P. H. Taylor, S. Yan, Q. W. Ma, and P. A. E. M. Janssen, "Did the Draupner wave occur in a crossing sea?" *Proceedings of the Royal Society A*, vol. 467, no. 2134, pp. 3004–3021, 2011.

[10] S. Haver, *The Draupner Rogue Wave, Rogue Waves 2000*, Ifremer, 2000.

[11] K. Dysthe, H. E. Krogstad, and P. Müller, "Oceanic rogue waves," *Annual Review of Fluid Mechanics*, vol. 40, pp. 287–310, 2008.

[12] B. Kinsman, *Wind Wave: Their Generation and Propagation on the Ocean Surface*, Dover Phoenix, Englewood, NJ, USA, 1984.

[13] T. Matsuno, "Quasi-geostrophic motions in the equatorial area," *Journal of the Meteorological Society of Japan*, vol. 4, pp. 25–43, 1966.

[14] F. Farassat and M. Farris, "The mean curvature of the influence surface of wave equation with sources on a moving surface," *Mathematical Methods in the Applied Sciences*, vol. 22, no. 17, pp. 1485–1503, 1999.

[15] J. L. Hammack, "A note on tsunamis: their generation and propagation in an ocean of uniform depth," *Journal of Fluid Mechanics*, vol. 60, no. 4, pp. 769–799, 1973.

[16] M. Duruflé and S. Israwi, "A numerical study of variable depth KdV equations and generalizations of Camassa-Holm-like equations," *Journal of Computational and Applied Mathematics*, vol. 236, no. 17, pp. 4149–4165, 2012.

[17] G. A. El, R. H. J. Grimshaw, and A. M. Kamchatnov, "Evolution of solitary waves and undular bores in shallow-water flows over a gradual slope with bottom friction," *Journal of Fluid Mechanics*, vol. 585, pp. 213–244, 2007.

[18] D. W. Pravica, N. Randriampiry, and M. J. Spurr, "Applications of an advanced differential equation in the study of wavelets," *Applied and Computational Harmonic Analysis*, vol. 27, no. 1, pp. 2–11, 2009.

[19] D. W. Pravica, N. Randriampiry, and M. J. Spurr, "Theta function identities in the study of wavelets satisfying advanced differential equations," *Applied and Computational Harmonic Analysis*, vol. 29, no. 2, pp. 134–155, 2010.

[20] D. Pravica, N. Randriampiry, and M. Spurr, "Reproducing kernel bounds for an advanced wavelet frame via the theta function," *Applied and Computational Harmonic Analysis*, vol. 33, no. 1, pp. 79–108, 2012.

[21] D. Pravica, N. Randriampiry, and M. Spurr, "q-Advanced sperical Bessel functions of the first kind and perturbations of the Haar wavelet," preprint, 2011.

[22] J. R. Holton, *An Introduction to Dynamic Meteorology*, Elsevier, Academic Press, San Diego, Calif, USA, 4th edition, 2006.

[23] A. E. Gill, *Atmosphere-Ocean Dynamics*, Academic Press, New York, NY, USA, 1982.

[24] T. S. Murty and Z. Kowalik, "Use of Boussinesq versus shallow water equations in tsunami calculations," *Marine Geodesy*, vol. 16, no. 2, pp. 149–151, 1993.

[25] E. -B. Lin and P. C. Liu, "A discrete wavelet analysis of freak waves in the ocean," *Journal of Applied Mathematics*, vol. 2004, no. 5, pp. 379–394, 2004.

[26] I. Daubechies, "The wavelet transform, time-frequency localization and signal analysis," *IEEE Transactions on Information Theory*, vol. 36, no. 5, pp. 961–1005, 1990.